SciTech, January 2016, San Diego, California

Wind Tunnel Manoeuvre Rig: A Multi-DOF Test Platform for Model Aircraft

Sergio A. Araujo-Estrada*
Department of Aerospace Engineering, University of Bristol, UK

Zheng Gong†
College of Aerospace Engineering,
Nanjing University of Aeronautics and Astronautics, Nanjing, China

Mark H. Lowenberg‡
Department of Aerospace Engineering, University of Bristol, UK

Simon Neild§
Department of Mechanical Engineering, University of Bristol, UK

Mikhail Goman¶
Department of Engineering, De Montfort University, Leicester, UK

This paper presents recent progress in the development of a novel multi-degree-of-freedom dynamic manoeuvre rig aimed at investigation of aircraft model nonlinear and time dependent aerodynamics in the wind tunnel. The purpose and characteristics of the rig are first described, along with a description of the data acquisition, processing and presentation system. The dynamic manoeuvre rig capabilities are demonstrated via a series of experiments involving a wind tunnel model aircraft in a closed section low-speed wind tunnel. First, an experiment illustrating low-speed wind tunnel aerodynamic model identification is presented. Then, examples of experiments involving real-time control of the rig/aircraft model are shown; these are evaluated in terms of testing productivity with a focus on the development and design of aircraft control laws.

I. Introduction

Efforts to gather information using large-scale static testing and forced oscillation techniques in wind tunnels have continued to this day[1] but the need for an enhanced motion experimental dynamic test bed has become apparent, both to physically simulate aircraft behaviour and to generate data for creating improved mathematical models of the unsteady aerodynamics.

The 'manoeuvre rig' concept was devised for these purposes: the intention was to provide for an aircraft model to be tested in up to five degrees of freedom (DOF) with motions imparted via its own control surfaces, and with an element of compensation applied to the rig dynamics so that the model behaves, in principle, as if it were in free motion under those DOFs. The resulting 'physical simulation' allows for the observation of aircraft behaviour, including the influence of nonlinear and/or time-dependent aerodynamics such as that responsible for the onset of upset/departure; and the motion data from such tests – or from forced motions driven by the rig compensator system – can then be used to carry out parameter estimation for mathematical

*PhD Student.
†Lecturer
‡Professor of Flight Dynamics, AIAA Senior Member.
§Professor in Nonlinear Structural Dynamics.
¶Professor, AIAA Senior Member.

model development. A couple of prototypes of the manoeuvre rig have been developed recently to obtain aerodynamic data from wind tunnel multi-DOF dynamic tests,[2] to characterise the oscillatory longitudinal pitch and heave motions of an aircraft model[3] and to numerically simulate free flight manoeuvres of a delta-wing aircraft model in a wind tunnel.[4]

This paper describes the rig and its features, including recent updates to allow for the improved controllability, updates to the software for real-time data acquisition and control tasks and some illustrative results. These results highlight the rig multi-DOF testing capability as well as the flexibility and simplicity to implement control algorithms with the new set-up. This research is aimed at extending ground testing capabilities for effective flight characteristics prediction, control law design and evaluation and increased testing productivity.

II. The Manoeuvre Rig

The new multi-DOF dynamic manoeuvre rig is an improved version of the one developed by Pattinson[5] as well as a continuing effort to further improve recent developments.[6] The principal enhancements are new instrumentation, an improved data acquisition and command electronics system, a new real-time data acquisition software system based on Python, the interfacing with Matlab Simulink and the replacement of the 2-DOF gimbal at the interface between the model and the front of the rig arm with a newly-designed 3-DOF gimbal, which requires the development of a new mathematical model. Additional modifications to the rig included a new IMU module, changes to the arm-roll measurement system, together with improvements to the compensator servos. Figure 1 shows the new rig layout along with a new 3-DOF model-gimbal. In Figure 1(a) a schematic diagram of the rig including the degrees of freedom and location of the two gimbals is presented. This is the layout after adding the 3-DOF model-gimbal, shown in Figure 1(b), which provides an additional model-roll DOF. The different parts that form the manoeuvre rig are described next.

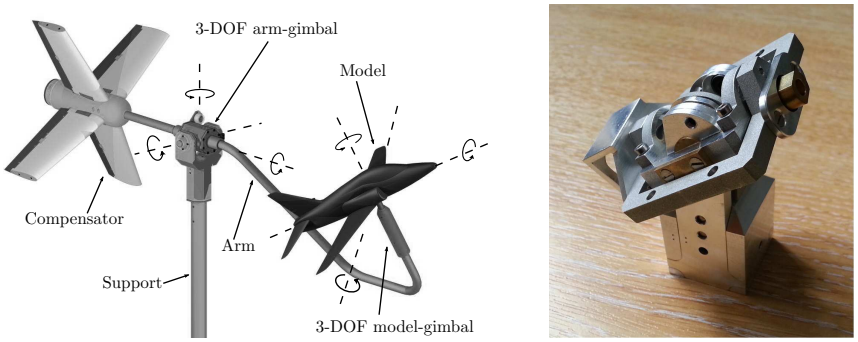

(a) The manoeuvre rig, new 6-DOF version

(b) A new 3-DOF gimbal has been installed to replaced the old 2-DOF version.[5]

Figure 1. The manoeuvre rig and the new 3-DOF gimbal.

The manoeuvre rig vertical support holds the 3-DOF arm-gimbal, which allows for arm-roll, arm-pitch and arm-yaw. The arm itself is made out of a 28 mm diameter steel tube, and supports the aerodynamic compensator on the rear end and the new 3-DOF model-gimbal at the front. The aerodynamic compensator consists of four identical wings in a cruciform layout, each of which possesses a control surface; a central body contains the compensator electronics. Additionally, a system to add different masses to counterbalance the model weight is built in at the back of the compensator. The 3-DOF model-gimbal sits at the front end. It allows for model-roll, model-pitch and model-yaw. The aircraft model is mounted on the 3-DOF model-gimbal. An approximate BAe Hawk aircraft model was used to carry out the experiments presented in this paper. A representation of the Hawk model mounted in the manoeuvre rig can be seen in Figure 1(a).

Figure 2 depicts the manoeuvre rig with the prototype Hawk model mounted in two of the University of Bristol's wind tunnels. In Figure 2(a) the rig is shown when installed in the 7' × 5' closed section wind tunnel. A safety cable system can be observed in the background: this is used to restrict the rig's motions. Figure 2(b) shows the rig mounted in the open-jet section wind tunnel.

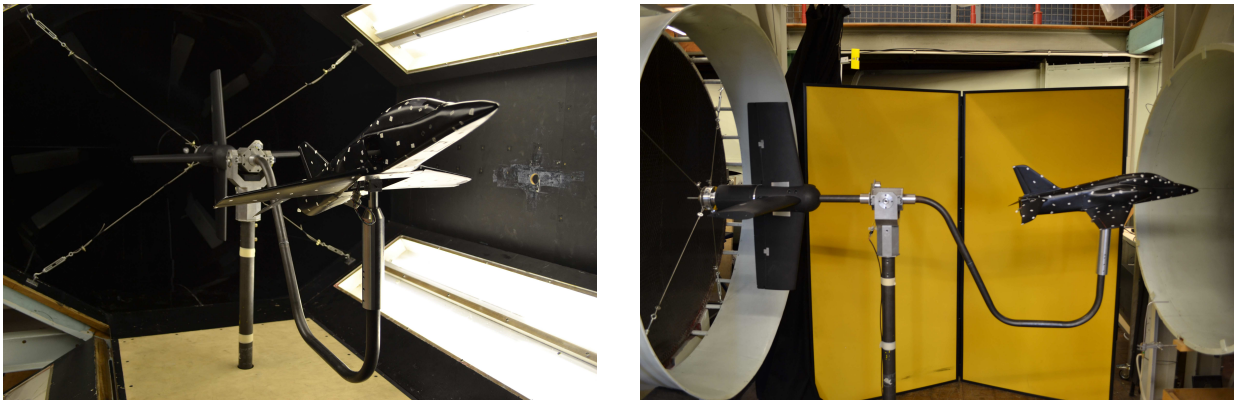

(a) 7' × 5' closed section wind tunnel.

(b) Open-jet section wind tunnel.

Figure 2. The manoeuvre rig mounted in two of the University of Bristol's wind tunnels.

The angular displacements of the 3-DOF arm-gimbal are measured using potentiometers. The angular displacements of the 3-DOF model-gimbal and the control surfaces from the compensator, are measured using absolute digital encoders. The angular displacements of the aircraft model control surfaces are measured using the potentiometers embedded in the servo motors; these were not measured in the previous version of the rig. All of these measurements are transmitted through an IEEE 802.11N WiFi network and collected by a PC acting as a software Access Point(AP).

A major component in the manoeuvre rig is the electronics subsystem. The main tasks of this subsystem are: transmitting and receiving data, recording signals from sensors and generating control signals to the servo motors. The previous electronics subsystem comprised three sets of boards: one inside the Hawk, one in the aerodynamic compensator and one at the ground station; it was developed by Pattinson and as he observed, there was room for improvement regarding its performance.[7] The previous three boards arrangement has been kept but a new electronics subsystem has been designed in order to improve the system capabilities and time latency.

In order to carry out the control of the rig for dynamic tests it is necessary for the electronic subsystem to be capable of real-time data acquisition. Previously conducted tests were limited to open-loop scenarios due to excessive time delay in data transmission/reception, as well as the absence of a means of directly measuring aircraft-model control surface displacements. The newly-designed data acquisition electronics system is a small scale integration module that includes an enhanced wireless data transmission and reception module, measures the displacement of the aircraft model control surfaces via the built-in potentiometers in its servos, acquires inertial data from an IMU mounted on the aircraft model, controls the motion of the aerodynamic compensator and aircraft model servos and measures the aircraft model angular motions. With the old 2-DOF model-gimbal the aircraft model angular motions were recorded using a pair of potentiometers, in the new 3-DOF model-gimbal, these were changed to digital encoders in order to improve quality and accuracy of the recorded signals.

At the core of the new subsystem lies a Microchip Technology Inc. dsPIC33E digital signal controller (DSC). In the DSC a time-triggered co-operative scheduler and message processing/sending system is running. It was developed to achieve time synchronization, real-time task execution and in-time message reaction/responding. By taking advantage of the Direct Access Memory (DMA) module and the Digital Signal Processing (DSP) engine available on the DSC, the sensor reading, servo control and message processing/sending tasks consume only 40µs, 70µs and 300µs respectively in each step, which translates into a 250Hz data sampling rate. In Figure 3(a) a diagram representing the different timing of tasks carried out by the DSC is shown.

The aircraft model and aerodynamic compensator servos are controlled using the DSCs in their respective control boards, which improves the accuracy and time response of the servos. This approach allows for direct measurement of the servo position and for approximate measurement of the controls surfaces position. The servo controller is implemented as a proportional plus derivative feedback positioning control. Instead of an integral component on the controller to reduce the steady state errors caused by coulomb friction on the

hinges, a nonlinear strategy was used. A Butterworth filter is implemented in the DSC to smooth the servo displacement reading and to compute the servo displacement rate. These computations use the DSP engine on the DSC which reduces the computational time.

An IEEE 802.11N WiFi network is established to allow communication between remote nodes - connected to the Hawk, the aerodynamic compensator and the ground station - and a PC node. XBee WiFi modules are used as remote nodes to establish the wireless network and embedded Universal Asynchronous Receiver/Transmitter (UART) modules running at 4 MBd are used to connect the Xbee WiFi modules to the DSCs. The PC node works as a software Access Point (AP) in the centre of a star network to collect all the transmitted data directly; by using this configuration a saving of up to 50% in transmission time is obtained when compared with a configuration using a hardware AP router which needs to redirect each data packet between nodes. A representation of the WiFi network structure is shown in Figure 3(b).

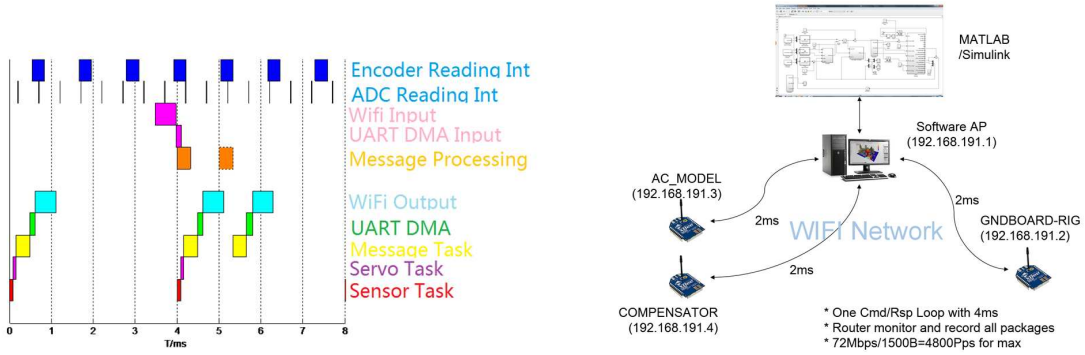

(a) DSC task scheduler.

(b) Wireless network structure.

Figure 3. The manoeuvre rig data acquisition system.

The implementation of a simplified Network Time Protocol (NTP) allows the DSCs connected to the remote nodes to synchronize the corresponding time computation with the PC node by measuring the relative time delay, time offset and shift time in idle state. Figure 4(a) shows the time latency distribution for a series of round-trip transmissions. The results from this experiment show that the time delay for node-to-AP communication is less than 4ms. The clock offset distribution is presented in Figure 4(b), it can be seen that the clock offset can be kept to within 100µs. Due to the low time latency, the tasks running on each DSC can be configured to be activated with milliseconds accuracy by the scheduler and messages from different DSCs can be sent in different time slices to avoid transmission collisions. This increased accuracy in time logging allows for the inclusion of 64 bit timestamps showing the generated time, sending time and received time in microseconds, in each transmitted message.

A software module was developed in Python - to run on a PC under Windows or Linux - to communicate, record, monitor and control the whole system and can be connected to a Matlab/Simulink environment via a User Datagram Protocol (UDP) communication link. Although neither Windows nor Linux are Real-Time Operating Systems and Python is not designed for real-time tasks, by introducing methods such as high priority application, multi-core parallel computing and by disabling garbage collection when processing data, the whole system achieves low time latency and in-time response capabilities. Figure 4(c) shows the command delay time history, from this plot it can be seen that on average the command delay is under 10 ms. Furthermore, if the command delay distribution is plotted, it can be observed that more than 96% of the transmitted commands arrive within 10 ms, as shown in Figure 4(d). The interconnection with a Matlab/Simulink environment facilitates the development of prototype control laws, as they can be first designed in Simulink and then tested by running hardware-in-the-loop experiments directly.

The previous 2-DOF gimbal via which the aircraft model was mounted to the end of the rig arm provided the aircraft model with its own pitch and yaw DOFs whereas rotation about the roll axis occurred at the arm-strut gimbal. Although this allowed the aircraft model a roll DOF, effective compensation for the arm moments of inertia and its offset centre of gravity (c.g.) was not feasible. The newly designed and manufactured 3-DOF model-gimbal incorporates an additional roll DOF at the model-arm interface. With this installed, 'natural' motion in the roll sense is possible. Representative physical simulation of the aircraft

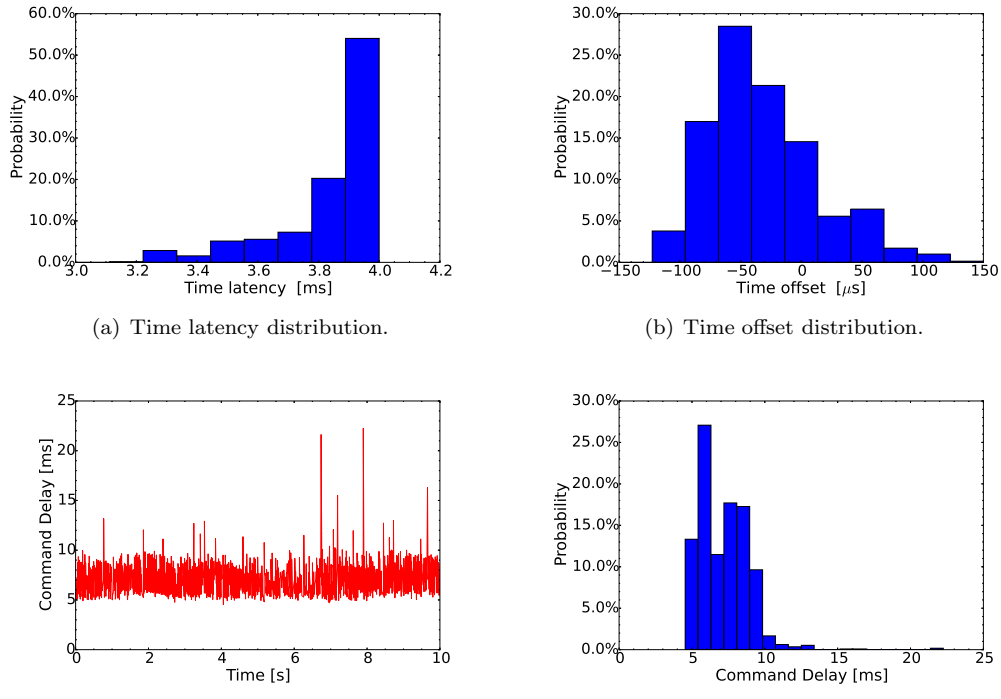

(a) Time latency distribution.

(b) Time offset distribution.

(c) Command delay time history.

(d) Command delay distribution.

Figure 4. Timing characteristics.

behaviour is therefore made easier since the control effort from the compensator control surfaces is reduced. A further significant benefit of adding the 3-DOF model-gimbal is the enhancement of the model motion envelope, thus the installation of the new gimbal should allow for tests closer to real flight conditions.

III. Experimental Capabilities

A screen shot of the manoeuvre rig Graphical User Interface (GUI) is presented in Figure 5. Three components of the GUI can be observed, namely the Access Point Centre (APC), the Sensors Output Graphical Display (SOGD) and the Cockpit Display System (CDS). The APC displays real-time information from data collected remotely; it serves as a simplified input interface for preprogrammed tasks, to control data recording and to monitor the overall health of the system. The SOGD main function is to present sensors information at reduced rate (currently the data is updated at a rate of 50Hz); it is also used to keep track of the amplitude of the motions developed by the system. The CDS is used to present information similar to that in the SOGD but in a closer format to what a glass cockpit configuration would present; it also has a higher update rate ($66 - 100$Hz).

Using the APC, various inputs can be applied to the aircraft model and aerodynamic compensator control surfaces. These inputs include steps, doublets, 3-2-1-1, ramps, sinusoidal linear frequency sweep as well as sinusoidal exponential frequency sweep. The input characteristics that can be defined using the APC include: start time, delta time, magnitude, sign and number of repetitions. If different, more complex inputs are required, these can be implemented using a Matlab/Simulink interface.

To demonstrate the rig capabilities a series of 1-DOF and 3-DOF experiments involving the Hawk model roll and pitch motions and the manoeuvre rig's arm roll motion were carried out in the 7' $\times$ 5' closed section wind tunnel at the University of Bristol. These experiments were carried out at a wind speed of 30 m/s. The experimental data was collected and recorded using the new software module and then post-processed using Matlab® and IPython. The reconfiguration process for the 3-DOF experiment took under 15 minutes and all the experiments were carried out in around three hours. To illustrate some of the manoeuvre rig applications, the experiments were divided into three categories: aircraft dynamic characteristics determination, testing

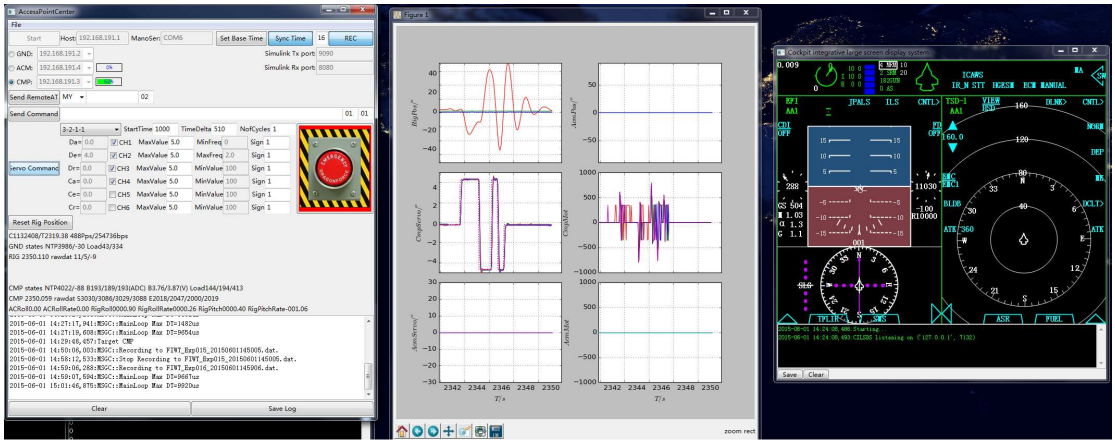

Figure 5. Manoeuvre rig graphical user interface screen shot.

envelope extension and aircraft control law evaluation.

A. Aircraft dynamic characteristics determination

To demonstrate the capabilities of the rig for determining aircraft dynamic characteristics an open loop 1-DOF aircraft roll experiment was carried out. The roll motion is provided by the model-gimbal: this DOF was not available in the previous version of the manoeuvre rig.[5] In this experiment the model-gimbal roll angle is equivalent to the aircraft roll angle. To estimate the aircraft model damping and control power effectiveness, two inputs to the aircraft model ailerons were used: a doublet and a 3-2-1-1 input. The inputs were applied using the APC. The amplitude of these inputs was limited to $\pm 4^\circ$ for the doublet input and $\pm 3^\circ$ for the 3-2-1-1 input. Additionally, both inputs were limited to the use of a 0.5 s delta time. These limits were necessary to avoid the aircraft model from reaching the mechanical limits of the model-gimbal, i.e., an aircraft model roll angle within a range of $\pm 42^\circ$.

Figure 6 shows the time histories of the Hawk model roll motion response to a doublet input followed by a 3-2-1-1 input to its ailerons. The time histories shown in Figure 6 correspond to two independent experiments, concatenated as indicated by vertical dashed lines appearing at $t \approx 3.5$ s in every plot. Figure 6(a) shows the time histories of both demanded and measured aircraft model aileron deflections. It can be seen that the measured aircraft model aileron deflections match the demanded deflections quite well. At the beginning and end of the experiment, aircraft aileron offsets can be seen. These offsets appear as the aircraft model aileron servos is switched off and no command is applied, remaining in a position held by inertial and friction forces, different from the demanded position.

Figure 6(b) shows the aircraft model roll rate time history. The minimum rate was $-153\,^\circ$/s, reached during the aileron doublet input. The maximum rate was $142\,^\circ$/s, this was attained during the aileron 3-2-1-1 input. Figure 6(c) shows the model-gimbal and hence aircraft model roll angle time history. The horizontal dashed lines in Figure 6(c) represent the physical limits of the roll motion aircraft-gimbal which are $\pm 42^\circ$. The maximum roll angle was 31.5° which was reached during the second half of the aileron doublet input. The minimum roll angle was -38.6°, encountered during the third part of the aileron 3-2-1-1 input.

From the time histories corresponding to the 1-DOF aircraft roll experiment shown in Figure 6, it can be seen that the allowable input delta time and magnitude are limited by the maximum allowable model-gimbal roll angle. To use a longer delta time and/or a larger magnitude, it is necessary to extend the testing envelope by increasing the allowable roll angle.

B. Extended testing envelope using manoeuvre rig

To extend the roll motion testing envelope, the arm roll DOF is released and a feedback control law to the arm compensator control surfaces implemented. The objective of the compensation feedback control law is to reduce the arm inertial effects and keep the model-gimbal roll angle within its physical limits. Ideally the model-gimbal roll angle should be kept as close as possible to zero - here the new model-gimbal roll

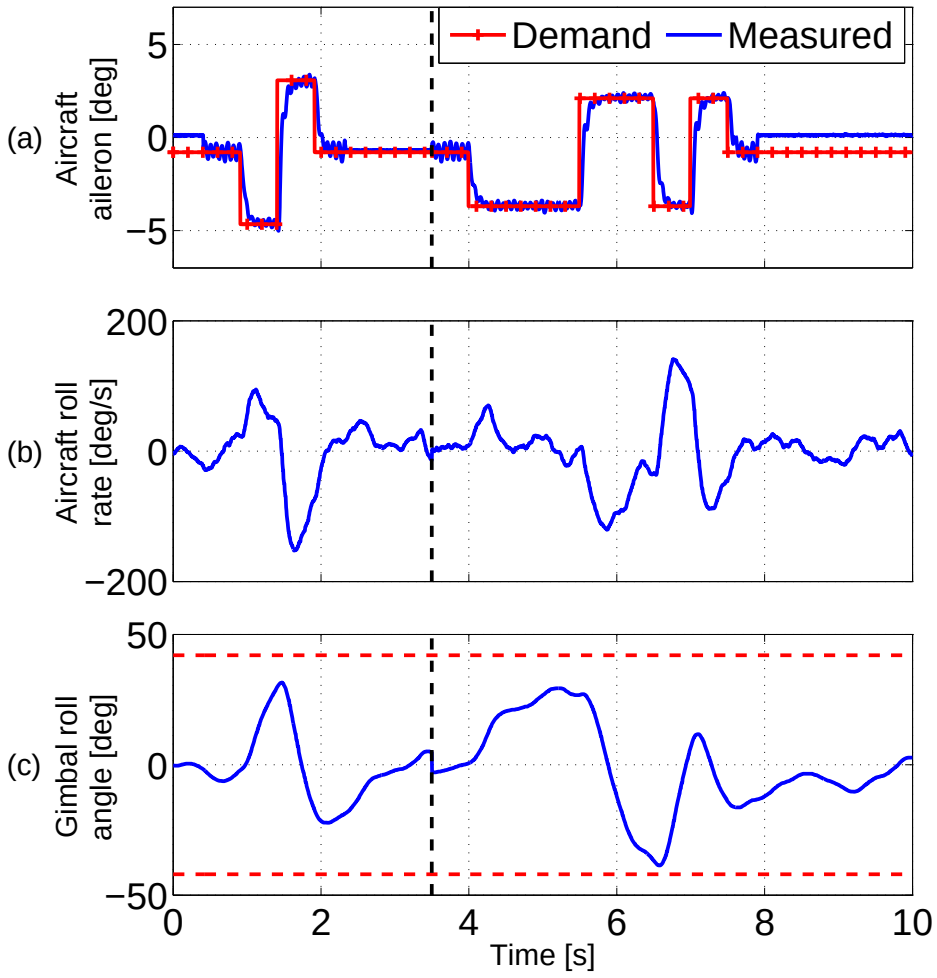

Figure 6. Hawk model roll motion response to a doublet input to its ailerons.

degree-of-freedom allows for error in this control objective as the data is valid provided the model-gimbal roll is kept to within $\pm 42°$.

For this experiment, the aircraft model was used in a open loop configuration, i.e. no feedback was used to control the motion of the aircraft. The manoeuvre rig was used in a 3-DOF configuration with aircraft roll, aircraft pitch and arm roll free to move. Although roll compensation could have been demonstrated using two degrees of freedom - aircraft model gimbal roll and arm roll - the additional model pitch degree of freedom was included in order to make the motions more interesting and to evaluate the system at higher angles of attack (not shown here). An input with similar characteristics to that of the 1-DOF test was applied to the aircraft ailerons to drive the roll motion, but it was applied for an extended period of time. To provide extended roll motion, the manoeuvre rig arm was used, with the aerodynamic compensator ailerons controlling the model-gimbal roll angle. The control law was implemented in Simulink®.

The characteristics of the aircraft aileron doublet input were as follows: the amplitude was $\pm 5°$, with a delta time equal to 11 s for the first half of the input and a delta time equal to 12 s for the second half. The aircraft aileron demand was changed from a trimmed state of $-1.5°$ to a constant state condition of $-6.5°$ following a linear rate profile of $-5\,°/s^2$ to limit the acceleration of the system. A similar rate profile (opposite sign) was used to transition from the minimum aircraft aileron deflection into the maximum aircraft aileron deflection. A rate profile of $-1.6\,° s^{-2}$ was used to transition from the maximum aircraft aileron deflection into a trimmed state; this aileron deflection rate reduction was necessary to achieve an integer number of revolutions of the manoeuvre rig's arm.

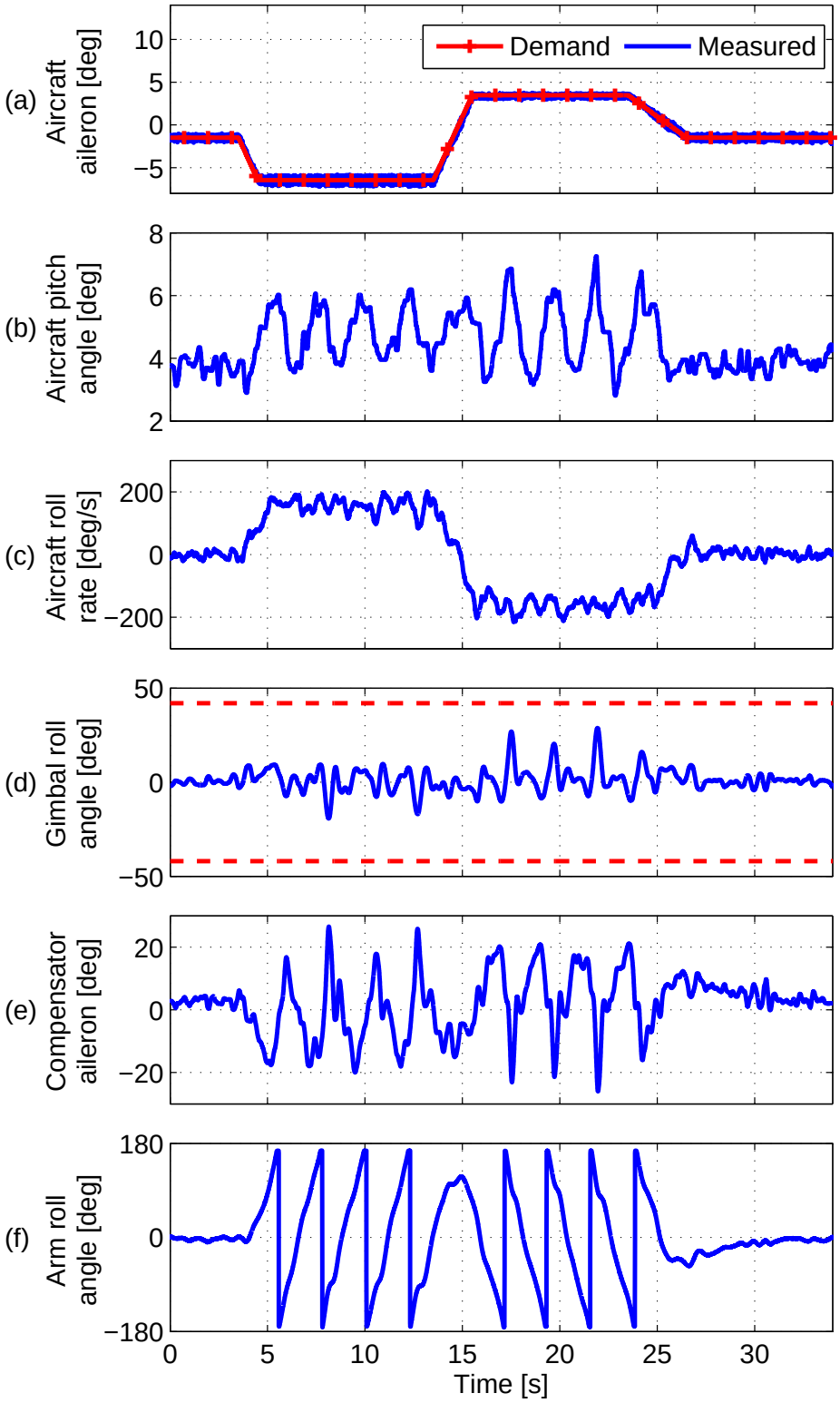

Figure 7. Hawk model roll motion response to a doublet input to its ailerons with roll compensation using manoeuvre rig.

Figure 7 shows the time histories of the Hawk model roll motion response to a doublet input to its ailerons with roll motion compensation using the manoeuvre rig. Figure 7(a) shows the time histories of both demanded and measured aircraft model aileron deflections. Figure 7(b) shows the aircraft model pitch angle time history. In this test the aircraft pitch angle is equivalent to aircraft angle of attack. Small changes in angle of attack can be seen in the aircraft model pitch angle plot in Figure 7(b); these fluctuations were in the range $-1^\circ \leq \Delta\alpha \leq 3^\circ$. Figure 7(c) shows the aircraft model roll rate time history. A quasi-steady roll rate of approximately $200\,^\circ/\mathrm{s}$ was achieved during this test. Figure 7(d) shows the model-gimbal roll angle time history. The horizontal dashed lines in Figure 7(d) represent the physical limits of the roll motion aircraft-gimbal, i.e., $\pm 42^\circ$. From the model-gimbal roll angle plot in Figure 7(d) it can be seen that the model-gimbal roll angle remained within the physical limits range throughout the entire test. The model-gimbal roll angle was bounded in the range $-20^\circ \leq \phi_{mg} \leq 30^\circ$.

Figure 7(e) shows the aerodynamic compensator aileron deflection time history. The aerodynamic compensator aileron deflection plot represents the control effort for roll motion compensation and deflections are well within its limits of $\pm 40^\circ$. Figure 7(f) shows the manoeuvre rig arm roll angle time history. The manoeuvre rig arm roll angle changes from 180° to -180° indicating continuous roll motion and the ability of the rig to extend the roll motion testing envelope. A total of four anticlockwise revolutions were completed during the negative deflection of the aircraft model aileron. During the positive deflection of the aircraft model aileron a further four clockwise revolutions were completed.

From the time histories corresponding to the 3-DOF aircraft roll, aircraft pitch and arm roll experiment shown in Figure 7, it can be seen that compensation feedback control law effectively reduced the arm inertial effects. Consequently the testing envelope was extended, this allowed the aircraft model to exhibit its full natural roll response, essentially as if it were in free flight in these degrees of freedom.

C. Evaluation of aircraft control laws using manoeuvre rig

The manoeuvre rig can also be used to develop and assess the performance of aircraft control laws. To demonstrate the capabilities of the rig for evaluation of aircraft control laws a 3-DOF experiment was carried out. In this 3-DOF experiment, as in Section III.B, the aircraft roll, aircraft pitch and arm roll DOFs were free to move and the remaining DOFs were fixed at neutral positions. Closed loop control was used to drive the aircraft ailerons to match the aircraft roll rate to the roll rate demand. To provide extended roll motion, the manoeuvre rig arm was used, with the aerodynamic compensator ailerons controlling the model-gimbal roll angle (as in Figure 7). Both control laws were implemented in Simulink®.

For this experiment, the characteristics of the roll rate demand were as follows: the amplitude was $\pm 430\,^\circ/\mathrm{s}$, with a delta time equal to 18.1 s for the first half of the roll rate demand and a delta time equal to 19.5 s for the second half. The roll rate demand transition - from zero to a positive steady state condition, from a positive to a negative steady state condition and from a negative steady state condition to zero - was changed following a linear acceleration profile of $107\,^\circ/\mathrm{s}^2$ to limit the acceleration of the system.

Figure 8 shows the time histories of the Hawk model roll closed loop motion response to a roll rate ramp-and -hold command with roll motion compensation using the manoeuvre rig. Figure 8(a) shows the time histories of the measured aircraft model aileron deflections. Figure 8(b) shows the aircraft model pitch angle time history. In this experiment the aircraft pitch angle is equivalent to the aircraft angle of attack. Small changes in angle of attack can be seen in the aircraft model pitch angle plot in Figure 8(b), within the range $-2.6^\circ \leq \Delta\alpha \leq 2.3^\circ$. Figure 8(c) shows both the demanded and the measured aircraft model roll rate time histories. A higher steady roll rate was achieved when compared to the experimental data shown in Figure 7(c), with a steady roll rate of approximately $330\,^\circ/\mathrm{s}$ achieved during this test. Figure 8(d) shows the model-gimbal roll angle time history. The horizontal dashed lines in Figure 8(d) represent the physical limits of the roll motion aircraft-gimbal, i.e., $\pm 42^\circ$. From the model-gimbal roll angle plot in Figure 8(d) it can be seen that the model-gimbal roll angle remained within the physical range throughout the entire test. The model-gimbal roll angles was bounded by $-34^\circ \leq \phi_{mg} \leq 28^\circ$. Figure 8(e) shows the aerodynamic compensator aileron deflection time history. The aerodynamic compensator aileron deflection plot represents the control effort for roll motion compensation and lies well within its deflection range of $\pm 40^\circ$. Figure 8(f) shows the manoeuvre rig arm roll angle time history. The manoeuvre rig arm roll angle changes from 180° to -180° indicating continuous roll motion. A total of twelve anticlockwise revolutions were completed during the negative deflection of the aircraft model aileron. During the positive deflection of the aircraft model aileron fifteen clockwise revolutions were completed. As in Section III.B, the manoeuvre rig with roll compensation allows the model to exhibit its natural roll response as if it were in free flight in these DOFs.

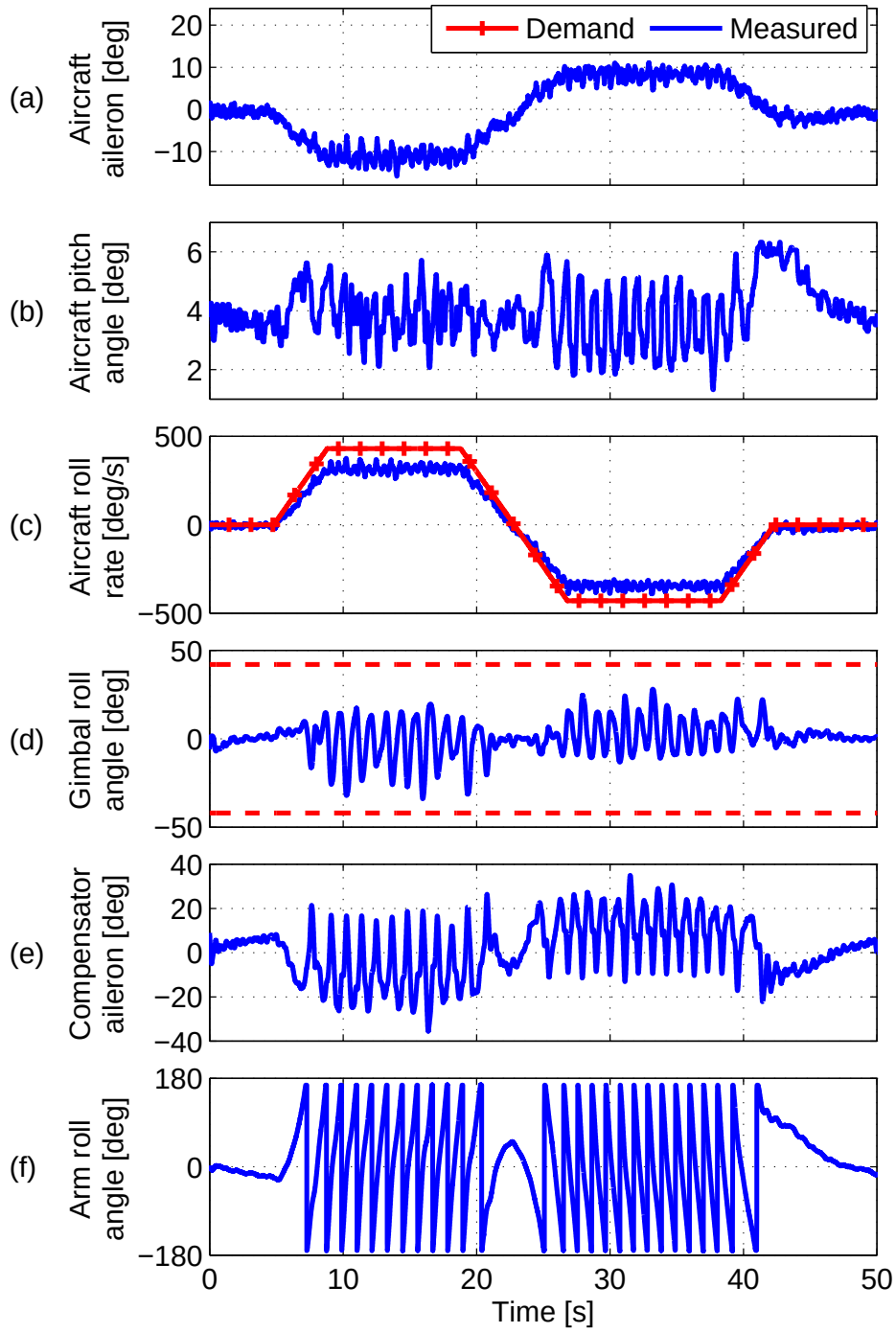

Figure 8. Hawk model closed loop response to a roll rate demand.

This technique allows the testing of velocity vector rolls commanded by the aircraft model ailerons.

The above examples illustrate the capabilities of the manoeuvre rig for flight characteristics prediction, for evaluation of aircraft control laws as well as the flexibility to carry out tests at different DOFs configurations. The short reconfiguration time along with the real-time data collection prove vital to increase testing productivity. The update of the data acquisition electronics subsystem, along with the new software module developed in Python have reduced time delays in the wireless transmission system. Together these updates

allow for improved wind tunnel testing quality.

IV. Concluding Remarks

In this paper a novel multi-degree-of-freedom dynamic manoeuvre rig designed to aid in the investigation of aircraft model high-angle-of-attack aerodynamics in the wind tunnel and the development of control laws has been presented. The addition of a new data acquisition electronics system, a 3-DOF model-arm gimbal, the implementation of a new real-time data acquisition software system and the interfacing to Matlab/Simulink®, all part of recent updates to the rig, were presented as part of current research. Recently carried out tests on the new version of the rig for the approximate BAe Hawk aircraft model were discussed, with results that demonstrate the purpose of the rig updates and show much-improved time latency.

The experimental determination of aircraft roll dynamic characteristics, enabled by the addition of an extra model body axes roll DOF, was demonstrated via a 1-DOF aircraft roll experiment. The testing envelope for the 1-DOF roll motion experiment was limited to $\pm 42^\circ$ of roll motion. The capability of the manoeuvre rig for multi-degree-of-freedom testing was exploited to extend the testing envelope of the 1-DOF roll motion experiment. By releasing aircraft model pitch DOF and the manoeuvre rig arm's roll DOF, the aerodynamic compensator ailerons were used to compensate the inertial effects of the rig's arm. The experimental results shown the compensation control law successfully maintained the aircraft model within the model-gimbal physical limits. Finally, the capability of the manoeuvre rig for aircraft control laws evaluation was demonstrated via a 3-DOF aircraft roll, aircraft pitch and arm roll experiment. In this experiment, a feedback control law in which the aircraft model followed a predetermined roll rate profile was implemented and tested. These results demonstrate the ability to physically simulate the aircraft model's natural behaviour, i.e., as if it were not supported in a rig in roll.

Acknowledgments

The authors would like to thank and acknowledge Mr Lee Winter from the University of Bristol wind tunnel laboratory, for his invaluable support and work during the refitting, assembly and modification of the equipment used to carry out the experiments presented in this paper.

S. A. Araujo-Estrada's research is supported by the Science and Technology National Council (CONACYT-Mexico), studentship # 215262. Z. Gong's research is supported by the China Scholarship Council(CSC) for one year study at the University of Bristol, scholarship # 201306835006. S. Neild is supported by an EPSRC fellowship (EP/K005375/1).

References

[1]Shah, G. H., Cunningham, K., Foster, J. V., Fremaux, C. M., Stewart, E. C., Wilborn, J. E., Gato, W., and Pratt, D. W., "Wind-Tunnel Investigation of Commercial Transport Aircraft Aerodynamics at Extreme Flight Conditions," *World Aviation Congress & Display*, SAE, Phoenix, Arizona, November 2002, SAE Technical Paper 2002-01-2912, DOI: 10.4271/2002-01-2912.

[2]Pattinson, J., Lowenberg, M. H., and Goman, M., "A Multi-Degree-of-Freedom Rig for the Wind Tunnel Determination of Dynamic Data," *AIAA Atmospheric Flight Mechanics Conference*, AIAA, Chicago, Illinois, August 2009, DOI: 10.2514/6.2009-5727.

[3]Pattinson, J., Lowenberg, M. H., and Goman, M., "Characterisation of wind tunnel observed, large-amplitude pitch limit-cycles," *AIAA Atmospheric Flight Mechanics Conference*, AIAA, Portland, Oregon, August 2011, DOI: 10.2514/6.2011-6526.

[4]Peyada, N. K., Gosh, A. K., and Go, M., "Mathematical modelling, simulation, and estimation of aircraft parameters using five degree-of-freedom dynamic test rig," *Proceedings of the Institution of Mechanical Engineers, Part G: Journal of Aerospace Engineering*, Vol. 226, No. 1, 2012, pp. 55–63, DOI: 10.1177/0954410011407265.

[5]Pattinson, J., Lowenberg, M. H., and Goman, M., "Multi-Degree-of-Freedom Wind-Tunnel Maneuver Rig for Dynamic Simulation and Aerodynamic Model Identification," *Journal of Aircraft*, Vol. 50, No. 2, 2013, pp. 551–566, DOI: 10.2514/1.C031924.

[6]Araujo-Estrada, S. A., Lowenberg, M. H., Neild, S., and Goman, M., "Evaluation of Aircraft Model Upset Behaviour Using Wind Tunnel Manoeuvre Rig," *AIAA Atmospheric Flight Mechanics Conference*, AIAA, Kissimmee, Florida, January 2015, DOI: 10.2514/6.2015-0750.

[7]Pattinson, J., *Development and Evaluation of a Wind Tunnel Manoeuvre Rig*, Ph.D. thesis, University of Bristol, Bristol, England, UK, 2010, Department of Aerospace Engineering.